

PARAMETRIC ANALYSIS ON REPEATED IMPACT-BASED CAPTURE OF A FREE-FLOATING CYLINDRICAL OBJECT BY A DUAL-ARM SPACE ROBOT

Naoki Hase¹, Kenji Nagaoka¹, Kazuya Yoshida¹

¹ *Tohoku University, Address:6-6-01 Aoba, Aramaki-aza, Aoba-ku, Sendai, Miyagi, 980-8579, Japan
E-mail:{naoki,nagaoka,yoshida}@astro.mech.tohoku.ac.jp*

ABSTRACT

This paper presents a parametric analysis on the repeated impact-based capture of a free-floating object by a dual-arm space robot toward future space debris removal missions. The dual-arm space robot encloses the target and enables the attenuation of rotational motion by repeated impact with the left and right arms. In particular, the dual arm enables the robot to compensate the undesired flicking of the debris by which one arm is controlled to track the debris' motion to maintain the repeated impact. Through this parametric analysis, we investigate the effect of the control parameters on the target capture.

1 INTRODUCTION

Debris satellites of stopped or failed operation are increasing on the earth orbit. To actively capture and remove such space debris, debris collection by an autonomous robot is considered.

Generally, space debris loses its attitude control function and involves a complex rotation. Hence, the space robot that performs the capturing operation needs to control the translational and rotational motion of the floating space debris by the contact. Hereafter, the space debris to be captured is called a target. With regard to this contact problem, studies pertaining to the control of translational and rotational motions have been advanced.

Previously, Kawamoto et al. [1] proposed a method of providing impulses to a rotating floating target by multiple contacts of a fixed ground manipulator, and converging rotations uniaxially. In addition, Nakanishi et al. [2] proposed the impedance control of the contact force and verified by simulation to stop the relative motion. These methods are premised on the contact with a single manipulator. A single manipulator cannot restore the target if the target is pushed away from the working range of the manipulator. Meanwhile, Takahashi et al. [3] simulated the capturing operation of rotating objects by a dual-arm space robot using a hybrid simulator. In this simulator, the robot was fixed on the ground, and the robot itself was not rotating. Herein, we aim to establish a method to control the motion through repeated impact with the target by appropriately controlling the velocity of the hand of a dual-arm space robot system as shown in Fig. 1. To realize the attenuation of the target motion, the dynamics and contact mechanics of the dual-arm space robot must be understood. Therefore, we first define the target capture models (the robot and the target) that conflict with each other, and organizes the dynamics of the dual-arm space robot. Subsequently, we describe the modeling of the contact force acting at the contact

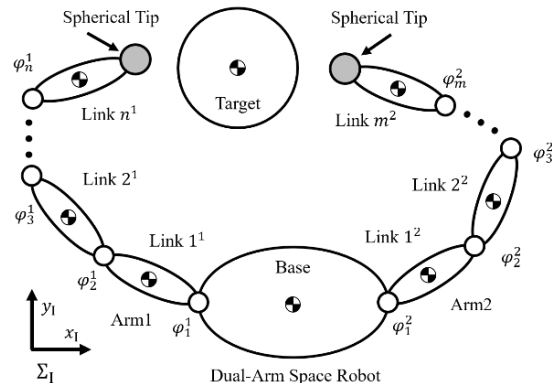


Fig. 1. Schematic View of Dual-Arm Space Robot and Target Model

between the hands of the dual-arm and the target. In addition, by repeatedly colliding the hand tip of the robot against the target surface, we discuss the control law that stabilizes from the attenuation of the target motion to the final stable capture state and verify using numerical simulation. The effect of the control parameters on the target capture is then investigated using parametric analysis. The space robot is assumed to have a mechanical compliant wrist [4] to simplify the normal contact force as a linear spring-damper model. Moreover, for the tangential contact force, a Coulomb friction model is applied.

2 DUAL-ARM SPACE ROBOT

2.1 Target Capture Model

Herein, the target capture model consists of a two-dimensional model of a robot and a target as shown in Fig. 1. The space robot has two arms mounted on the robot body and spherical rigid tips attached on them. Moreover, the inertial coordinate system is defined as Σ_1 . The following are the assumptions for the modeling.

- The gravity acceleration is zero.
- The robot base and the target are rigid bodies.
- The mass, moment of inertia, and center of mass of the robot are known.
- The target is a circular rigid body, and its center of mass is positioned at the geometrical center.
- The target's radius, center of mass position, and velocity are known.

2.2 Basic Equation of a Dual-Arm Space Robot

For the dual-arm model, the suffix k in the upper right of each variable indicates the arm number. The key variables used in the robot model are defined as follows.

$\mathbf{H}_b \in \mathbf{R}^{6 \times 6}$: Inertia matrix of the robot base

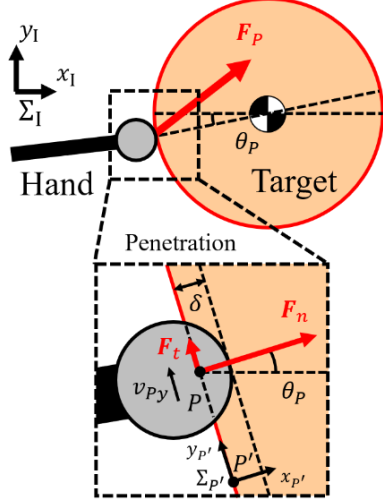


Fig. 2. Contact Force Model of Manipulator's End-Effector and Rigid Target

$\mathbf{H}_m^k \in \mathbf{R}^{n^k \times n^k}$: Inertia matrix of the arm k
 $\mathbf{H}_{bm}^k \in \mathbf{R}^{6 \times n}$: Interference inertia matrix of the base and the arm k
 $\mathbf{x}_b \in \mathbf{R}^6$: Center of mass position of the base
 $\boldsymbol{\varphi}^k \in \mathbf{R}^{n^k}$: Joint angle of the arm k
 $\mathbf{c}_b \in \mathbf{R}^6$: Velocity nonlinear term of the base
 $\mathbf{c}_m^k \in \mathbf{R}^{n^k}$: Velocity nonlinear term of the arm k
 $\mathbf{F}_b \in \mathbf{R}^6$: External force acting on the base
 $\boldsymbol{\tau}^k \in \mathbf{R}^{n^k}$: Torque acting on the joint of the arm k
 $\mathbf{J}_b^k \in \mathbf{R}^{6 \times 6}$: Jacobian matrix on the base
 $\mathbf{J}_m^k \in \mathbf{R}^{6 \times n^k}$: Jacobian matrix on the arm k
 $\mathbf{F}_h^k \in \mathbf{R}^6$: External force acting on the tip of the arm k
 Unless otherwise specified, each variable shall be defined in Σ_1 . The equation of motion of the dual-arm space robot can be expressed as follows.

$$\begin{bmatrix} \mathbf{H}_b & \mathbf{H}_{bm}^1 & \mathbf{H}_{bm}^2 \\ \mathbf{H}_{bm}^{1T} & \mathbf{H}_m^1 & \mathbf{0}_{n^1 \times n^2} \\ \mathbf{H}_{bm}^{2T} & \mathbf{0}_{n^1 \times n^2} & \mathbf{H}_m^2 \end{bmatrix} \begin{bmatrix} \ddot{\mathbf{x}}_b \\ \dot{\boldsymbol{\varphi}}^1 \\ \dot{\boldsymbol{\varphi}}^2 \end{bmatrix} + \begin{bmatrix} \mathbf{c}_b \\ \mathbf{c}_m^1 \\ \mathbf{c}_m^2 \end{bmatrix} = \begin{bmatrix} \mathbf{F}_b \\ \boldsymbol{\tau}^1 \\ \boldsymbol{\tau}^2 \end{bmatrix} + \begin{bmatrix} \mathbf{J}_b^{1T} & \mathbf{J}_b^{2T} \\ \mathbf{J}_m^{1T} & \mathbf{0}_{6 \times n^1} \\ \mathbf{0}_{6 \times n^2} & \mathbf{J}_m^{1T} \end{bmatrix} \begin{bmatrix} \mathbf{F}_h^1 \\ \mathbf{F}_h^2 \end{bmatrix} \quad (1)$$

3 CONTACT DYNAMICS MODEL

As shown in Fig. 2, let P be the contact point of the arm hand of the robot and the target and \mathbf{F}_P the contact force vector acting on the contact point. In general, as a contact mechanics model between rigid bodies, the contact force \mathbf{F}_P can be expressed by a function of the virtual penetration δ and its velocity $\dot{\delta}$ as follows.

$$\mathbf{F}_P = f(\delta, \dot{\delta}) \quad (2)$$

Here, as a free-floating system, the contact force normal to the contact surface can be simulated by assuming a simple linear spring-damper model. Herein, we also model the contact force with a linear spring-damper model. Given that the contact surface has a stiffness coefficient of k_p and a viscosity coefficient of c_p , \mathbf{F}_P is expressed as follows:

$$\mathbf{F}_P = k_p \delta + c_p \dot{\delta} \quad (3)$$

Here, the contact force acting on the target is defined as the resultant force \mathbf{F}_P of the normal contact force \mathbf{F}_n and the tangential one \mathbf{F}_t to the tangent plane. In the tangential direction, a frictional force acts. As shown in Fig. 2, a coordinate system $\Sigma_{P'}$ with the origin P' near the contact point P is defined, where the $y_{P'}$ axis is parallel to the tangential direction of the contact surface and the $x_{P'}$ axis is orthogonal to the $y_{P'}$ axis. Furthermore, the unit vectors of $x_{P'}$ and $y_{P'}$ are given as $\mathbf{e}_{P'x}$ and $\mathbf{e}_{P'y}$, respectively. Given the linear spring-damper model, \mathbf{F}_n acting on the contact point is expressed as follows:

$$\mathbf{F}_n = (k_p \delta + c_p \dot{\delta}) \cdot \mathbf{e}_{P'x} \quad (4)$$

where k_n and c_n are the stiffness and viscous damping coefficient in the normal direction, respectively. With respect to the tangential direction, the sliding friction is assumed to occur during contact. The frictional force is defined as Coulomb's friction model. Given that μ is the dynamic friction coefficient of the contact and the relative sliding velocity at the contact point is v_{py} , \mathbf{F}_t acting on the contact point is given as follows.

$$\mathbf{F}_t = -\text{sgn}(v_{py}) \mu |\mathbf{F}_n| \cdot \mathbf{e}_{P'y} \quad (5)$$

where $\text{sgn}(v_{py})$ is a sign function given by

$$\text{sgn}(v_{py}) = \begin{cases} 1 & v_{py} > 0 \\ 0 & v_{py} = 0 \\ -1 & v_{py} < 0 \end{cases} \quad (6)$$

Furthermore, the contact force \mathbf{F}_P ($\mathbf{F}_n, \mathbf{F}_t$) is expressed in $\Sigma_{P'}$ ($x_{P'}, y_{P'}$). If the target is smooth and circular, the direction of the contact force is determined by the angle θ_p regardless of the target attitude. Eqs. (7) and (8) express the normal direction force and the tangential direction force.

$$\mathbf{F}_n = \begin{cases} |\mathbf{F}_n| \cos \theta_p \\ |\mathbf{F}_n| \sin \theta_p \end{cases} \quad (7)$$

$$\mathbf{F}_t = \begin{cases} -\text{sgn}(v_{py}) \mu |\mathbf{F}_n| \sin \theta_p \\ -\text{sgn}(v_{py}) \mu |\mathbf{F}_n| \cos \theta_p \end{cases} \quad (8)$$

Accordingly, the contact force in Σ_1 is derived as follows.

$$\mathbf{F}_P = \begin{bmatrix} |\mathbf{F}_n| \{ \cos \theta_p - \text{sgn}(v_{py}) \mu \sin \theta_p \} \\ |\mathbf{F}_n| \{ \sin \theta_p - \text{sgn}(v_{py}) \mu \cos \theta_p \} \end{bmatrix} \quad (9)$$

4 REPEATED IMPACT USING PATH-TRACKING CONTROL

In this section, we introduce the control law that can achieve the final stabilized capture by the repeated impact of the hand tips of the robot on the target surface. The contact force model is fundamental for the capture problem via contact with a rotating floating target. Generally, in motion damping via contact, after the impact, the target's translational motion is suppressed by the damping effect of the normal force and its rotational motion by the torque resulting from the tangential friction force. Herein, we propose a method that can suppress the relative motion of the target and move to a safer capture operation by repeating the impact with a dual-arm robot. In this method, we establish a unified control framework from the motion damping to capture the target by performing continuously repeated impact. To realize the

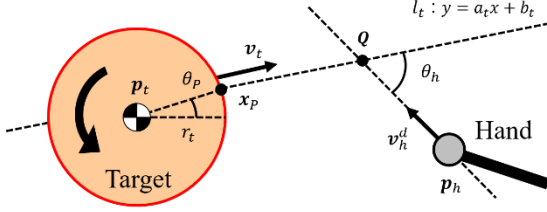


Fig. 3. Path-Tracking Control Model for Robot Arm to Target Motion

repeated impact by a dual-arm space robot, the hand velocity must be appropriately controlled such that the target does not deviate from the workable area of the dual arm. In this section, we first derive a target path-tracking control law with the aim of realizing repeated impact according to the relative motion to the target. Subsequently, the repeated impact-based capture sequence of a floating target with rotation motion is presented based on the tracking control.

4.1 Target Path-Tracking Control

Fig. 3 shows the schematic diagram of the target path-tracking control. By predicting the target motion direction from the center of mass velocity of the target, this control method enables the arm tips to reach a confluence point on the path of which the target will traverse, before the target reaches it. The path-tracking control is set to be executed only while the dual-arm and the target are not in contact. Further, while performing the path-tracking control, the other arm stops operating, and the base attitude control of the robot is not considered.

The target path-tracking control law is achieved step by step as shown below.

1. The contact point angle θ_p and path-tracking angle θ_h are set.
2. The predicted path l_t of the target motion is calculated from the center of mass position and velocity of the target, the radius, and the contact point angle θ_p .
3. Based on the tip position of the robot arm, the predicted path l_t , the path-tracking angle θ_h , and the confluence point Q of the tip and the target are calculated.
4. The hand velocity norm of the robot arm is calculated to reach the confluence point before the target reaches it.
5. Using the values of the path-tracking angle θ_h and the hand velocity norm, the desired hand velocity v_h^d is derived.

Here, the target center of mass position and velocity in Σ_I are defined as $p_t = [x_t \ y_t]^T$ and $v_t = [\dot{x}_t \ \dot{y}_t]^T$, respectively. The target radius is defined as r_t , and the hand position and velocity are defined as $p_h = [x_h \ y_h]^T$ and $v_h = [\dot{x}_h \ \dot{y}_h]^T$, respectively. Furthermore, given that the confluence point is defined as $Q = [x_Q \ y_Q]^T$, the angle of the contact point from the target center of mass in Σ_I is defined as the contact angle θ_p as shown in Fig. 3, and the angle between the predicted path and the target hand velocity is defined as θ_h . The path-tracking control

law is derived based on the procedure above. First, the slope a_t and intercept b_t of the target path are expressed as follows:

$$a_t = \frac{\dot{y}_t}{\dot{x}_t} \quad (10)$$

$$b_t = \begin{cases} (y_t + r_t \sin \theta_p) - a_t(x_t + r_t \cos \theta_p) & : x_h > x_t \\ (y_t - r_t \sin \theta_p) - a_t(x_t - r_t \cos \theta_p) & : x_h < x_t \end{cases} \quad (11)$$

where $\dot{x}_t \neq 0$ and $\dot{y}_t \neq 0$. Here, the intercept of Eq. (11) is expressed as a position on the target circumferential surface, which is shown as an intercept of the predicted path passing through the target contact position x_p . Further, in the dual-arm space robot, as the contact is established alternately by the left and right arms, the contact position is expressed in two ways. From Eqs. (10) and (11), the predicted path l_t is obtained as follows:

$$y = a_t x + b_t \quad (12)$$

Next, to calculate the confluence point for the arm tip, the slope and intercept of the target path of the arm are calculated. Given that the inclination of the target path is a_h , the following relationship is given:

$$\tan \theta_h = \frac{a_h - a_t}{1 + a_h a_t} \quad (13)$$

Hence, the slope can be calculated as follows.

$$a_h = \frac{a_t + \tan \theta_h}{1 - a_t \tan \theta_h} \quad (14)$$

Further, from the current arm hand position vector p_h and a_h , the intercept of the linear equation of the target path is given by

$$b_h = -a_h x_h + y_h \quad (15)$$

In this study, the desired path of the hand is given as follows:

$$y = a_h x + b_h \quad (16)$$

By simultaneously solving equations Eq. (12) and (16), a confluence point at which the arm tip should reach is obtained as the intersection point of two straight lines. Here, each component of the point Q becomes the following Eq. (17) using a_t , a_h , b_t , b_h .

$$\begin{cases} x_Q = \frac{b_h - b_t}{a_t - a_h} \\ y_Q = \frac{a_t b_h - a_h b_t}{a_t - a_h} \end{cases} \quad (17)$$

Here, the time until the hand reaches the point Q is expressed using p_h , v_h , and Q ; the time until the contact point of the target reaches Q is expressed using x_p , v_t , and Q . Consequently, the following condition equation needs to be satisfied.

$$\frac{\|Q - p_h\|}{\|v_h\|} \leq \frac{\|Q - x_p\|}{\|v_t\|} \quad (18)$$

The target hand velocity norm satisfying Eq. (18) is expressed by

$$\|v_h^d\| = k_h \frac{\|Q - p_h\|}{\|Q - x_p\|} \|v_t\| \quad (19)$$

where k_h is a constant and the arm tip can reach the confluence point Q before the target does when $k_h \geq 1$. Eq. (20) expresses $\|v_h^d\|^2$ by using each component.

$$\|v_h^d\|^2 = \dot{x}_h^2 + \dot{y}_h^2 \quad (20)$$

Here, as the gradient a_h of the target path can be written as $a_h = \dot{y}_h / \dot{x}_h$, by substituting it into Eq. (20), each component of the target hand velocity can be obtained as

follows:

$$\begin{cases} \dot{x}_h^d = \pm \frac{1}{\sqrt{1+a_h^2}} \|\mathbf{v}_h^d\| \\ \dot{y}_h^d = \pm \frac{a_h}{\sqrt{1+a_h^2}} \|\mathbf{v}_h^d\| \end{cases} \quad (21)$$

Because the sign of the arm hand velocity is determined by the positional relationship between the center of mass of the target and the hand tip, the desired hand velocity \mathbf{v}_h^d based on the sign is determined as Eq. (22).

$$\mathbf{v}_h^d = \begin{bmatrix} \frac{1}{\sqrt{1+a_h^2}} \|\mathbf{v}_h^d\| & \frac{a_h}{\sqrt{1+a_h^2}} \|\mathbf{v}_h^d\| \end{bmatrix}^T \quad (22)$$

Next, the relationship between the desired hand velocity of each arm, including the angular velocity will be considered [5]. The arm's angular velocity $\boldsymbol{\omega}_h^{k,d}$ is set to $\mathbf{0}$ to avoid fluctuations in the angle of the tip while the arm is tracking the target. Further, the other arm stops its operation and yields $\mathbf{0}$ as the hand velocity. Subsequently, the desired hand velocity $\dot{\mathbf{x}}_h^{k,d}$ of each the arm is expressed by Eqs. (23)-(26) according to the situation of the arm.

- In the case of target tracking by the left arm

$$\dot{\mathbf{x}}_h^{1,d} = [\mathbf{v}_h^{1,dT} \quad \mathbf{0} \quad \dots \quad \mathbf{0}]^T \quad (23)$$

$$\dot{\mathbf{x}}_h^{2,d} = [\mathbf{0} \quad \dots \quad \mathbf{0}]^T \quad (24)$$

- In the case of target tracking by the right arm

$$\dot{\mathbf{x}}_h^{1,d} = [\mathbf{0} \quad \dots \quad \mathbf{0}]^T \quad (25)$$

$$\dot{\mathbf{x}}_h^{2,d} = [\mathbf{v}_h^{2,dT} \quad \mathbf{0} \quad \dots \quad \mathbf{0}]^T \quad (26)$$

Here, the hand velocity is summarized as $\dot{\mathbf{x}}_h = [\dot{\mathbf{x}}_h^{1,T} \quad \dot{\mathbf{x}}_h^{2,T}]^T$.

4.2 Capture Sequence by Repeated Impact

In this section, the capture sequence for a rotating free-floating target by a dual-arm space robot is introduced using the path-tracking control.

1. Both hands of the robot move with a constant initial velocity and reduce the distance between the hands until either hand contacts the target.
2. After the impact, the path-tracking control is performed along the calculated target path.
3. At the starting contact, the dual-arm is stopped, and the target velocity and angular velocity are suppressed using the damping effect of the normal force of Eq. (4) and the torque resulting from the friction force of Eq. (5).
4. After the impact, path-tracking control is performed by another arm.
5. Repeat sequence 2 to 4 until both hands are simultaneously contacting with the target and become the final capture state.
6. When the two hands are in contact with the target simultaneously, the capture is completed.

The sequence of the target capture by repeated impact is shown in Fig. 4. By controlling the robot arm with the sequence above, the safe capture of the target can be realized using the repeated impact without precisely controlling the contact force. In particular, the path-

tracking control enables the repeated impact to be maintained without the target deviating from the workable area of the robot arm. Therefore, the motion suppression and capture of the target can be realized by the common control framework. Moreover, because this control method does not explicitly use the information of the inertia characteristics and the surface physical characteristics (contact surface rigidity, friction) of the target, it is an effective capture method even when the target information cannot be accurately estimated.

5 VALIDATION BY SIMULATION

5.1 Simulation Model

In the simulation, the dual-arm model is assumed to have three links for each arm. Let the target model be a circular rigid body with the center of mass at the center of the circle. Fig. 5 and Tab. 1 show the model and link parameters of the robot and the target used in the simulation, respectively. Here, the wrist compliance mechanism also used in the previous research of our research group is assumed to define the parameters of the contact point [6]. The mechanism mounted on each arm's hand tip is a sphere with diameter $d = 0.2$ [m], stiffness coefficient $k = 900$ [N/m], and viscous damping coefficient of the contact $c = 6$ [N · s/m]. The dynamic friction coefficient is $\mu = 0.1$.

5.2 Simulation Conditions

In the initial condition of the numerical simulation shown in Tab. 2, the two hands were brought close to each with velocities \mathbf{v}_h^1 , \mathbf{v}_h^2 , to capture the target rotating with an initial angular velocity ω_t . Further, for simplicity, the initial position of both hands was set on a straight line passing through the center of mass of the target.

6 PARAMETRIC ANALYSIS SIMULATION

In the target capture simulation, the contact angle was set to $\theta_p = 0$. As the control parameters, we used the following: $\theta_h = 90, 85, 80, 75, 70, 65, 60, 55, 50, 45$ [deg], $K_h = 1, 3, 5, 7, 9, 11, 13, 15, 17, 19, 21$, and $V_h = 0.05, 0.1, 0.15, 0.2, 0.25, 0.3$ [m/s].

Tab. 1. Link Parameters of Simulation Model

	Mass [kg]	Inertia [kg · m ²]	Length [m]
Base	7.695	0.09783	$l_{b1}=0.32$ $l_{b2}=0.22$
Link1 ¹	0.570	0.001777	0.1910
Link2 ¹	0.570	0.001777	0.1910
Link3 ¹	0.560	0.006761	0.0619
Link1 ²	0.570	0.001777	0.1910
Link2 ²	0.570	0.001777	0.1910
Link3 ²	0.560	0.006761	0.06109
Target	3.550	0.003583	$r_t=0.1$

Tab. 2. Initial State Value

Symbols	Value
$\boldsymbol{\varphi}^1$ [deg]	$[78 \quad -90 \quad -78]^T$
$\boldsymbol{\varphi}^2$ [deg]	$[-78 \quad 90 \quad 78]^T$
\mathbf{v}_h^1 [m/s]	$[V_h \quad 0]^T$
\mathbf{v}_h^2 [m/s]	$[-V_h \quad 0]^T$
\mathbf{v}_t [m/s]	$[0 \quad 0]^T$
ω_t [rad/s]	3

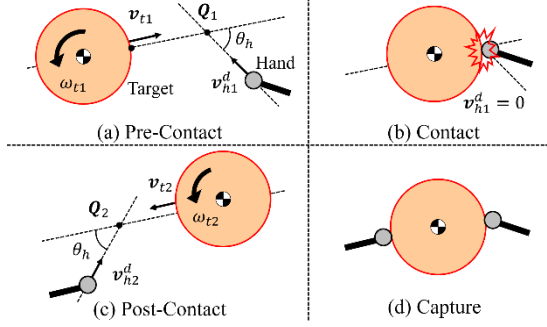


Fig. 4. Capture Sequence by Proposed Control Method Using Repeated Impact

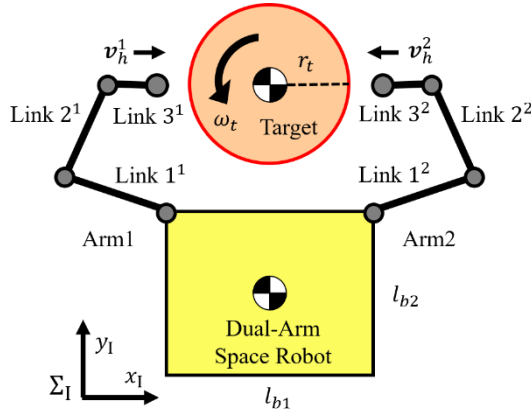


Fig. 5. Simulation Model of Space Robot with Dual-Arm and the Target

6.1 Simulation Results

The three representative simulation results are shown in Figs. 6–11. The results of the three cases as follows:

- Case 1: $\theta_h = 80$, $K_h = 13$, $V_h = 0.1$ (getting away from the base)
- Case 2: $\theta_h = 75$, $K_h = 1$, $V_h = 0.05$ (collision with the base)
- Case 3: $\theta_h = 65$, $K_h = 7$, $V_h = 0.25$ (capture)

Figs. 6, 8, and 9 are the snapshots of the typical examples of each case. Figs. 7, 9, and 11 are the time histories of the angular velocity of the robot base and the target. The detailed discussion is shown below.

6.1.1 Case 1 (Getting Away from the Base)

Fig. 6 confirms that the repeated impact is achieved. However, as shown, the left hand does not reach the target approximately 14 s after the start of the simulation. Further, from Fig. 7, it is understood that the left hand does not reach the target before the target angular velocity is sufficiently suppressed. Based on the conservation of the momentum, the translational motion of the robot and the target occurs after the collision. If the translational motion of the target is large, the target traverses to the extent that the arm does not reach. Subsequently, the arm of the robot enters a singular point. In this case, the left arm enters the singular point before the angular motion of the target is sufficiently attenuated. Hence, if the robot can sufficiently attenuate the motion of the target within

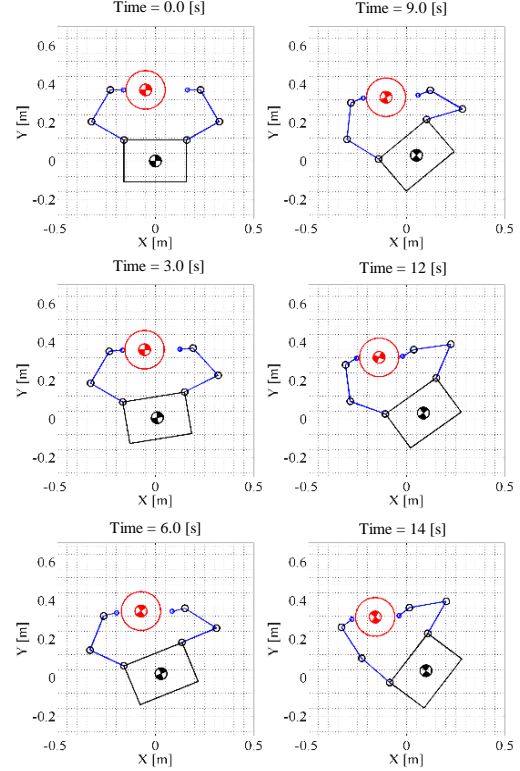


Fig. 6. Snapshots of simulation result in Case 1

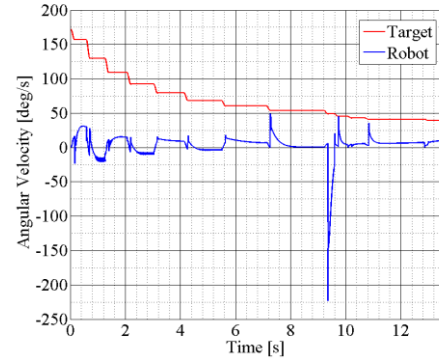


Fig. 7. Time history of target's angular velocity in Case 1

an appropriate time, we can convert the angular momentum of the whole system before distributing it to the translational motion.

6.1.2 Case 2 (Collision with the Base)

As shown in Figs. 8 and 9, although the repeated impact is achieved, the target is pushed in the direction of the base collision. This is because of the slow tracking velocity of the hand and the translational velocity of the target in the direction toward the base when the hand contacts at points above the center of mass of the target in Σ_I .

6.1.3 Case 3 (Capture)

Fig. 10 that the repeated impact is accomplished, and the target capture is finally completed approximately 4 s after

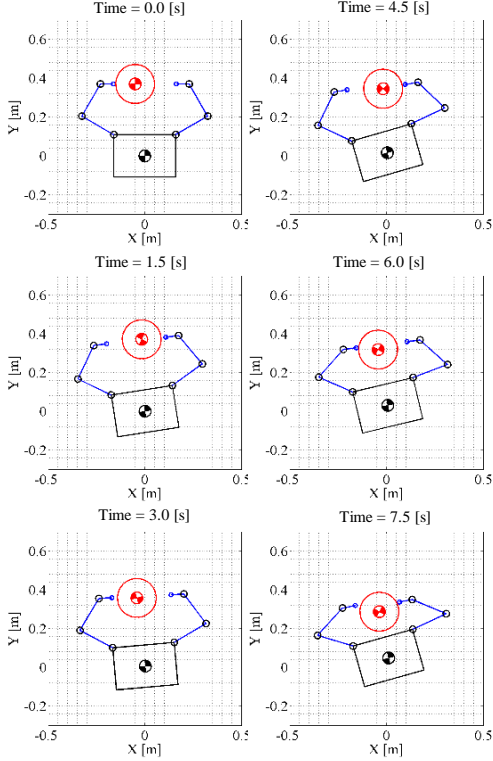


Fig. 8. Snapshots of simulation result in Case 2

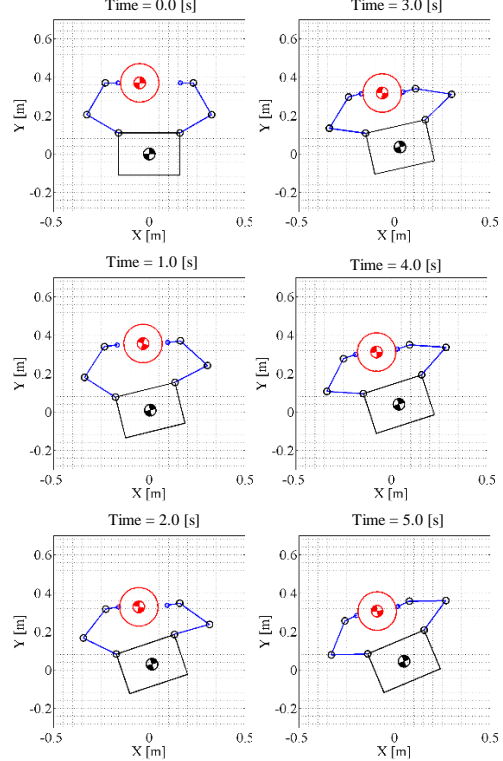


Fig. 10. Snapshots of simulation result in Case 3

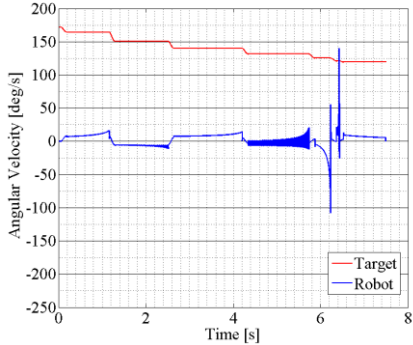


Fig. 9. Time history of target's angular velocity in Case 2

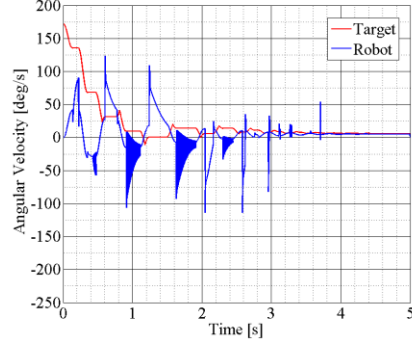


Fig. 11. Time history of target's angular velocity in Case 3

the start of the simulation. This is because the hand velocity also becomes effective in the direction of reducing the distance between the hands. Fig. 11 shows the time histories of the angular velocity of the target and the base of the robot. The result confirms that the time until the motion convergence is shorter than that of Case 1 and 2. Further, the base of the robot and the target rotational motion converges at a constant velocity after the capture owing to the repeated impact. Because the target is rotating in the initial state, the whole system after the capture performs a rotational motion in accordance with the preservation of the angular momentum.

Cases 1, 2, and 3 show that the motion suppression of the target is possible without controlling the force during contact using the repeated impact.

6.2 Parametric Analysis of Capture Simulation

The parametric analysis results of repeated impact are shown in Figs. 12-17, and Tab. 3. In each case, green indicates that the target is captured successfully, red indicates that the target collides with the base of the robot, and orange indicates that one arm does not reach the contact point and one arm enters a singular point. As the initial hand velocity increases, the conditions for capturing (green) increases. Further, the conditions in which the target collides with the base (red) is often shown when the tracking velocity ratio K_h of the hand is small, and this number increases as the initial hand velocity increases. We will discuss the parametric analysis below.

First, when the path-tracking angle θ_h is smaller than

90°, we confirmed that the hand velocity is applied in a direction that reduces the distance between the hands and the capture can be easily performed. In addition, we found that when θ_h is 65°, the number of captures accomplished is the largest. If θ_h is larger than 65°, the velocity in the direction to shorten the distance between both hands is small, therefore the interval of the repeated impact becomes larger. When the interval of contact with the target is small, the target moves outside the operation area of the arms, so it becomes difficult to capture. If θ_h is too small, the confluence point is set inside the target, and the contact force at one impact becomes too large. If the contact force is too large, the target is pushed away from the operation area of the arms. Therefore, we concluded that θ_h needs to be changed to shorten the distance between both hands without giving a large contact force to the target.

Regarding the path-tracking velocity ratio K_h , the larger the tracking velocity, the easier it is to move the hand to the contact point. Further, the hand contacts with the target to converge the velocity in the vertical direction, as shown from the barycentric coordinate system of the robot base, rendering it is easy to capture. However, if K_h is too large, the base moves in a reactionary motion. Subsequently, the hand cannot remain at the confluence point and the contact point shifts. In addition, if K_h is too small, the hand collides with the target before it reaches the confluence point. Therefore, because it is necessary to place the hands on the path of the center of mass to attenuate the target motion, we concluded that K_h needs to be changed according to the target velocity and the relative position between the target and the robot hand.

Regarding the initial hand velocity V_h , the larger the V_h , the larger is the contact force to the target and the frictional force; therefore, the rotational motion and capture are easier to attenuate. If V_h is too small, the rotational motion of the target attenuated by a single impact becomes small, hence requiring more time for attenuation. Subsequently, either one of the arms does not reach the target owing to the rotational motion of the robot itself. In addition, if V_h is too large, the rotational motion of the target to be attenuated by one impact increases, however, the translational velocity of the target and the robot increase and the tracking velocity of the hand also increases. As the velocities of the target and the hands increase, the hands push away the target. Therefore, an appropriate V_h must be chosen to yield the translational velocity of the target, such that the repeated impact can be maintained within the movable range of the arm.

From the above, we concluded that the appropriate control parameters must be selected to allow the target to maintain the repeated impact in the operation area and to perform sufficient motion damping.

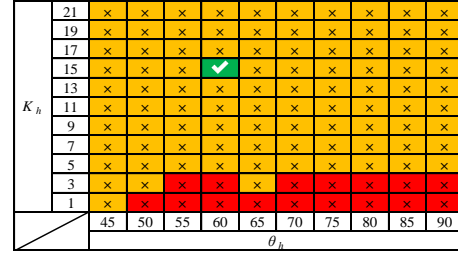


Fig. 12. Simulation Result in Case of $V_h = 0.05$

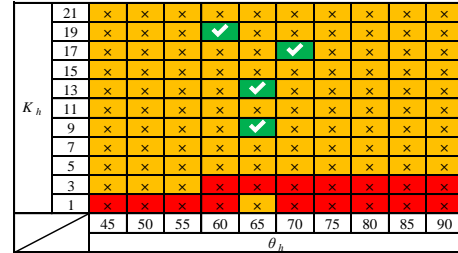


Fig. 13. Simulation Result in Case of $V_h = 0.10$



Fig. 14. Simulation Result in Case of $V_h = 0.15$



Fig. 15. Simulation Result in Case of $V_h = 0.20$

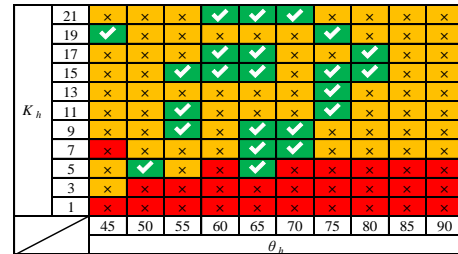


Fig. 16. Simulation Result in Case of $V_h = 0.25$

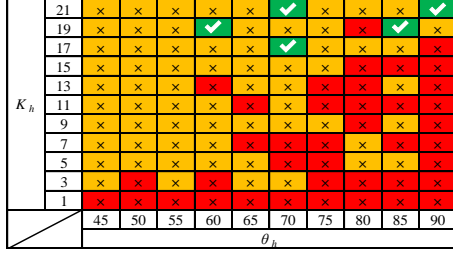


Fig. 17. Simulation Result in Case of $V_h = 0.30$

Tab. 3. Cases of simulation result

✓	Success : Catch
x	Failure : Getting away from the base
x	Failure : Collision on the base

7 CONCLUSION

In this study, we derived the path-tracking control of the target to realize its capture by repeated impact using a dual-arm space robot. This control system shows the process of calculating the desired hand velocity using the current hand position, the desired contact point with the target, and the conditional expression of the time to reach the contact point. In this simulation verification, after the description of the path-tracking control parameters, we confirmed that the target motion can be attenuated without controlling the contact force. Further, the motion attenuation and the capture by the repeated impact method can be achieved continuously by the path-tracking control. In addition, we analyzed how each parameter influences the ease of capturing the target in the motion attenuation process.

References

- [1] S. Kawamoto, S. Kitagawa, and K. Matsumoto, Angular Momentum Reduction Using Mechanical Impulse for Uncontrollable Satellite Capturing, *The Journal of Space Technology and Science*, Vol. 18, No. 2, pp. 225-231, 2002.
- [2] H. Nakanishi, N. Uyama, and K. Yoshida, Virtual Mass of Impedance System for Free-Flying Target Capture, in *Proc. 2010 IEEE/RSJ Int. Conf. on Intel. Rob. Syst.*, pp. 4101-4106, 2010.
- [3] R. Takahashi, H. Ise, A. Konno, and M. Uchiyama, Hybrid Simulation of a Dual-Arm Space Robot Colliding with a Floating Object, *Proceeding of the 2008 IEEE International Conference on Robotics and Automation*, pp. 1201-1206, 2008.
- [4] N. Uyama, H. Nakanishi, K. Nagaoka, and K. Yoshida, Impedance-Based Contact Control of a Free-Flying Space Robot with a Compliant Wrist for Non-Cooperative Satellite Capture, in *Proc. 2012 IEEE/RSJ Int. Conf. on Intel. Rob. Syst.*, pp. 4477-4482, 2012.
- [5] Y. Umetani and K. Yoshida, Control of Space Manipulators with Generalized Jacobian Matrix, *Space robotics: dynamics and control*, edited by U. Xu and T. Kanade, Kluwer Academic Publisher, pp. 165-204, 1993.

- [6] N. Uyama, Y. Fujii, K. Nagaoka, and K. Yoshida, Experimental Evaluation of Contact-Impact Dynamics between a Space Robot with Compliant Wrist and a Free-Flying Object, *Proceeding of the 11th International Symposium on Artificial Intelligence, Robotics and Automation in Space*, #3B-4, 2012.